# Optimal Control of a Cascaded Inverter by Genetic Algorithm

**Houria Smail[1] and Amar Maafa[1]**

[1] LISEA Laboratory, Faculty of Applied Sciences, University of Bouira, Bouira 10000, Algeria.

E-mail: h.smail@univ-bouira.dz - omaafa@univ-bouira.dz

***Abstract:*** *This paper presents an approach to control cascaded inverters that are used in wind systems. The objective of the proposed approach is to minimize the total harmonic distortion (THD) of the output voltage of cascades H-Bridge inverters, by optimally selecting the switching angles. To test the performance of the approach used, different levels of cascaded H-bridge (CHB) inverters have been considered (5-level, 7-level and 11-level. The effectiveness of the proposed approach is evaluated with intensive simulations. The simulation results, carried out using MATLAB software, showed that the approach developed in this study allows a reduction of up to 35.61% in the total harmonic distortion, compared with the results obtained in the literature. In addition, the developed approach can be applied to any number of levels.*

*Keywords: Cascaded inverters; Harmonic distortion; Distortion factor; Wind energy; Static Compensator*

## Nomenclature list

| | |
|---|---|
| *a0, an, bn* | Fourier series coefficients |
| *Bijk* | Control signal of the switch "k", phase "j" and HBM "i" |
| *F* | Frequency (Hz) |
| *Fijk* | Connection function of the switch "k", phase "j" and HBM "i" |
| *Fobj* | Objective function |
| *I* | Current |
| $I_{1ij}$ | The output current in branch *1* of HBM "*i*" phase "*j*" |
| $I_{2ij}$ | The output current in branch *2* of HBM "*i*" phase "*j*" |
| $I_{sij}$ | The source current of HBM "*i*" phase "*j*" |
| $K_i$ | Coefficients |
| $K_{ijk}$ | The switch number "*k*" in phase "*j*" and HBM "*i*" |

| | |
|---|---|
| $M$ | The number of levels |
| $P$ | Active power |
| $Q$ | Reactive power |
| $s$ | The number of HBM by phase |
| $U_{AB}, U_{BC}, U_{CA}$ | Line to line voltages |
| $V$ | Voltage |
| $V_{1eff}$ | rms value of the fundamental component |
| $V_{an}, V_{bn}, V_{cn}$ | Phase voltages |
| $V_{dc}$ | Direct voltage source |
| $V_{dci}$ | Direct voltage source of HBM number "$i$" |
| $V_{eff}$ | rms value of the output voltage |
| $V_{ij}$ | Output voltage of HBM number "$j$" phase "$i$" |
| $w$ | Angular velocity (rad/s) |
| $X$ | Reactance |
| $\alpha_i$ | The switching angle of the first switch ($K_{ij1}$) of HBM number "$i$" |
| $\delta$ | Phase angle |

# 1. Introduction

The state of the power system regarding operational reserves may result in the islanding of certain sections due to the severity of the disruption[1]. In order to prevent such events, the operators of the electrical system impose, in the grid code, requirements on the quality and the form in which the power must be delivered to the system [2]. To satisfy the requirements for grid interconnection, the renewable energy resources (RER) like wind must offer grid operators the ability to provide reactive power support. Using power electronics, Flexible Alternative Current Transmission System (FACTS) devices have the capability of adjusting terminal voltage by managing the quantity of reactive power introduced into or extracted from the power system. When system voltage is low, the FACTS generates reactive power. When system voltage is high, it absorbs reactive power. The Static Synchronous Compensator (STATCOM) is one of the key FACTS devices. Based on a voltage-sourced converter, the STATCOM regulates system voltage by absorbing or generating reactive power.

It is well known that, three-phase multi-level inverter is the most important part of STATCOM. Hence, high number of voltage levels let the FACTS devices give a high quality voltage. Thanks to the appearance of significant methods inin power electronics, various voltage-source converters are developed, such as neutral-point clamped (NPC), modular multilevel converter, flying capacitor and cascaded multilevel inverter [3].

The role of power electronics is to control the energy conversion at the machine level and to transfer the converted power to the network [4]. The structures of multilevel converters ensure the distribution of the constraint in tension on various medium or low voltage switches while improving the waveforms (harmonic spectra) of the quantities of output [5]. Due to its modularity structure, cascade H-bridge inverter is one of the most preferred for high voltage transmission.

The important design consideration to enhance the output quality of any inverter is to minimize the total harmonic distortion (THD). Optimization techniques have been widely applied in control systems. A hybrid optimization approach combining Proximal Policy Optimization and the Slime Mold Algorithm, was introduced in [6], whereas a fuzzy-logic-based path planning framework for mobile robots was proposed in [7]. For harmonic elimination purposes, various control strategies and effective optimizations have been proposed. Some literatures propose new topologies of cascaded H-bridge multilevel inverter to generate large number of levels with a smaller number of components [8]. In [9], authors propose new topology with reduced number of switching which results in smaller size and low implementation cost. Power losses that occur during switching are also minimized in this architecture. In addition, we can find optimization methods that are applicable to other domains. To maximize the efficiency of a standard telesurgery system, the authors of [10] adopt a cascade control strategy. The central optimization for a master-slave type of teleoperation system is based on a new soft tissue model [11]. In [12], two-stage approach is used to developing a networked autonomous electric bus, utilizing both discrete-time and continuous-time optimization techniques.

By using two low frequency switches, Ponnambalam et al. proposed new symmetrical cascaded multilevel inverter to diminish the number of switches and hence the THD is reduced [13]. The number of switches can be reduced by using an asymmetrical cascaded half H-bridge multilevel inverter MLI, which was introduced in [14]. This is accomplished by selecting the input DC source values and connections in the appropriate manner. An elimination of the requirement for a polarity generation circuit is possible with the suggested topology.

As a result, the number of switches that need a high blocking voltage is decreased. Others focused their research on finding the optimum switching angles [15] to eliminate higher order harmonics and working on various methods such as Pigeon Inspired Optimization (PIO) [16], Particle Swarm Optimization (PSO) [17], and BAT algorithm [18]. A comparative study among various strategies was led in [19] and [20], with reference to total harmonic distortion in the output voltage. In [21], a Genetic Algorithm optimization was used to determine the switching angles for a cascaded multilevel inverter utilizing identical DC sources. However, the proposed method was limited to eliminate certain number of higher order harmonics (5th and 7th order). The modulation index range also limited, and the algorithm must be executed as many times as the number of solutions necessary to cover the entire modulation index range.

In this article, a new algorithm based on GA is proposed to reduce the percentage of total harmonic distortion applied to a seven-level cascaded H-bridge inverter. This approach aims to minimize the THD (total harmonic distortion) of the output voltage by acting on the switching angles and the modulation index.

Section 2 of this paper explains the impact of three-phase wind turbine operation under its own protection in the network. Section 3 presents the principle of operation of static compensation of the reactive power. The structure and the modelling operation of cascaded H-bridge inverter are presented in the section 4. The measurement of harmonic distortion and the proposed approach are described in detail, respectively in sections 5 and 6. Simulation results produced with MATLAB are illustrated in the section 7, followed by conclusion and results discussion in section 8.

# 2. Three-phase wind turbine induction generator

In this part of the paper, we will highlight the impact of the intermittent nature of the wind on the power generated by a wind farm using Sim power system toolbox. Figure 1 shows the Wind Turbine Induction Generator (WTIG) which uses squirrel-cage induction Generators.

As shown in the figure, the stator winding is connected directly to the grid and the wind turbine (WT) drives the rotor. The energy captured by the wind turbine is transformed into electrical power by the induction generator and conveyed to the grid via the stator winding. The pitch angle is regulated to restrict the generator's output power to its nominal value under elevated wind speeds. To produce electricity, the induction generator's speed must exceed the synchronous speed.

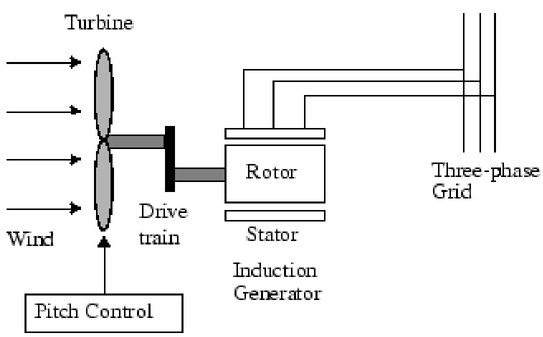


Figure 1
Wind turbine induction generator

To examine the impact of the WT operation into the network, we have considered the system given in Figure 2. The wind farm consists of three pairs of 1.5 MW WTIG. The wind farm is connected to a 25 kV, 60 Hz distribution system that exports power to a 120 kV grid through a 25 km line.

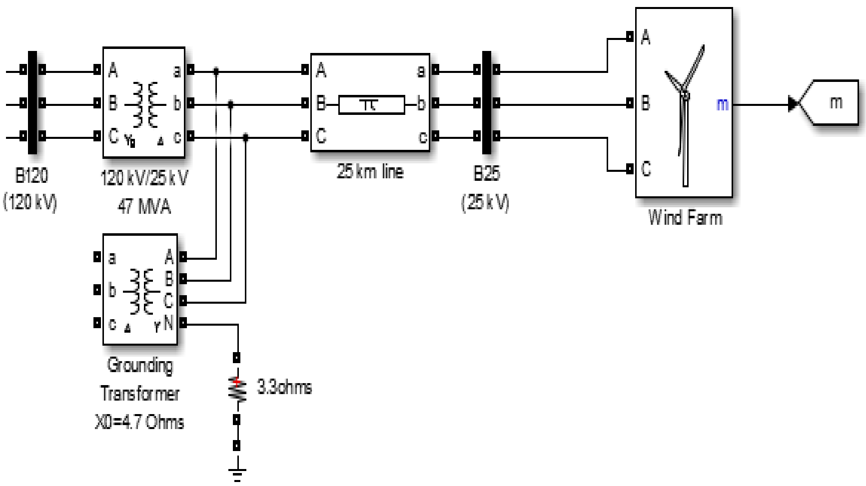


Figure 2:
Phasor simulation of a 9-MW wind farm using induction generator

The WT model is phasor model that allow transient stability type studies with long simulation times. The system is observed during 20 s through simulations in MATLAB environment using the Simulink and Sim power system toolbox.

The WT characteristics are shown in Figure 3. The graph shows the mechanical power of the turbine as a function of speed at wind speeds between 4 and 10 m/s. At 1 pu= 3 MW, the nominal mechanical power is produced by a nominal wind speed (WS) of 9 m/s. Each WT has a protection system monitoring voltage, current and machine speed.

The protection delays are set to 0.1 s, 10 s and 5 s, respectively, for voltage, current and speed.

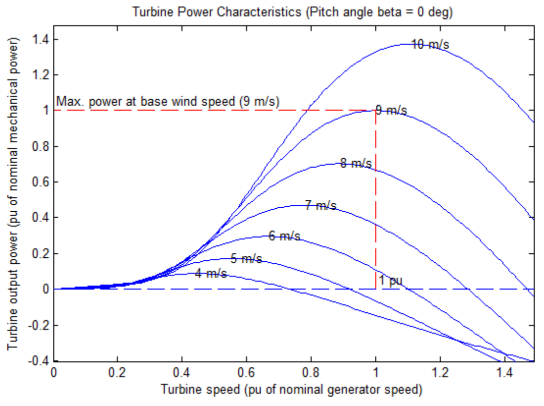


Figure 3
Turbine power characteristics (Pitch angle beta = 0 deg)

To examine the power absorption and dynamic response of the turbine under wind-wave conditions, we considered the wind profile given in Figure 4. Initially, the WS is set to 8 m/s for the three pairs of wind turbines. Then the WS is ramped in, 3 s after, to 11 m/s starting at $t = 2$ s for the first pair of WT, at $t = 4$ s for the second and at $t = 6$ s for the third pair of WT.

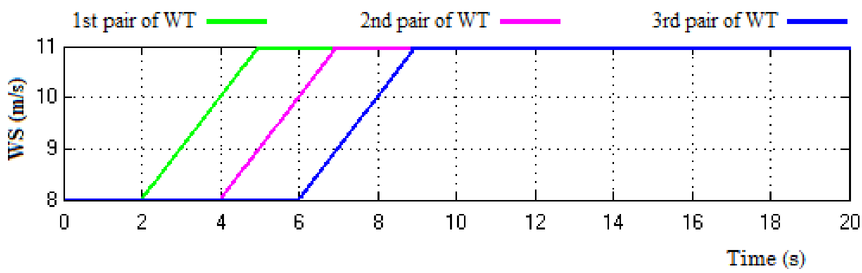


Figure 4
WS profile

The simulation results are given in Figure 5. The results show that for each pair of wind turbines, the generated active power starts increasing smoothly (together with the WS) to reach its rated value of 3 MW in approximately 8 s. The absorbed reactive power increases as the generated active power increases. The current at low voltage bus in the first pair of turbines is beyond the maximum set to 1.1 pu for more than 10 s.

This caused the trip of the first pair of WT at $t = 13.43$ s. The trip has been initiated by the AC overcurrent protection.

Due to the lack of reactive power support, the voltage at bus B25 drops to 0.91 pu. Then, it went back up when the turbine was tripped.

To maintain the 25 kV voltage at bus B25 close to 1 pu, it is immensely important to install a compensator device. In section 3, power-electronics based FACTS that is used to maintain the power system stability is presented.

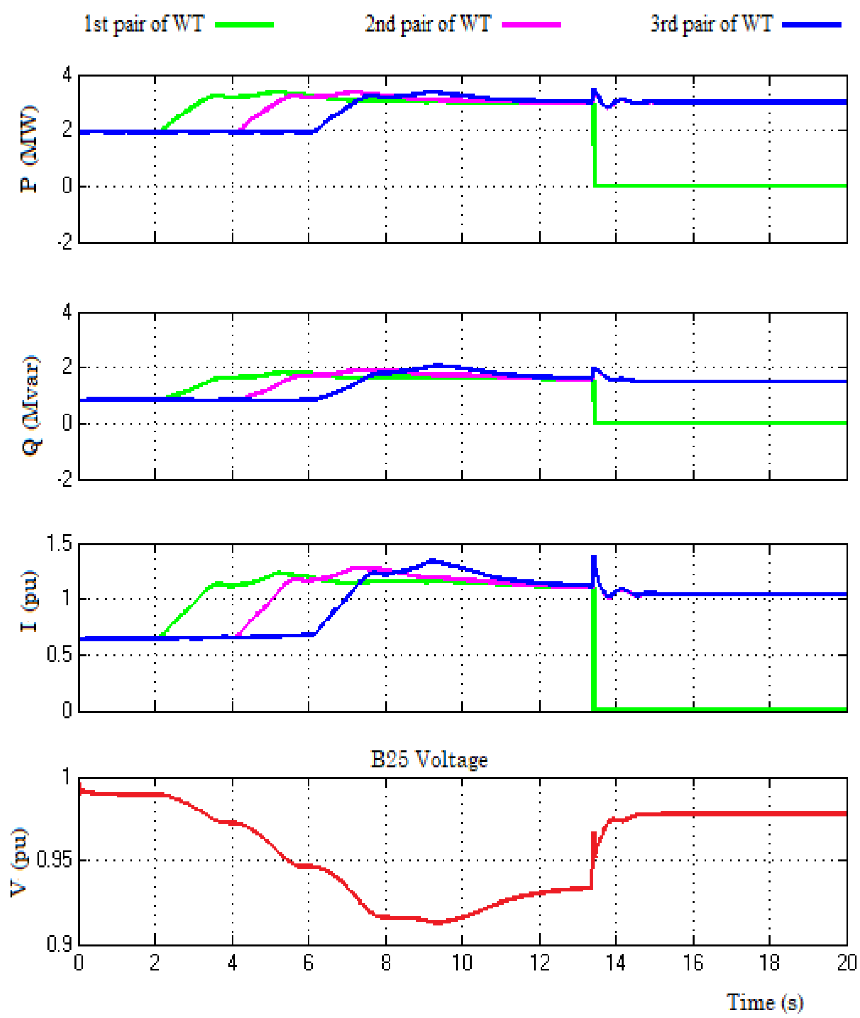


Figure 5

Impact of the WT operation on the network.

## 3. Static compensation of the reactive power

Static synchronous compensators are one of the main tools for managing reactive power. The STATCOM is a shunt device that belongs to the FACTS family of devices. It uses power electronics to regulate power flow and make power grids more stable during transients. The principle of its operation is explained on Fig. 6.

The modulation of reactive power is executed by a voltage-sourced converter (VSC) linked to the secondary side of a coupling transformer.. The VSC converts a direct current (DC) input voltage into a synthesized voltage output using forced-commutated power electronic devices such as GTOs, IGBTs, or IGCTs. V1 is the voltage of the system that needs controlling, and V2 is the voltage that the VSC produces. The equations that follow describe the transmission of active and reactive power from source V1 to source V2:

$$P = \frac{V_1 V_2 \sin\delta}{X} \tag{1}$$

$$O = \frac{V_1 (V_1 - V_2 \sin\delta}{X} \tag{2}$$

Where, X is the reactance of interconnection transformer, δ is the phase angle between V1 and V2, P is the active power and Q the reactive power.

In steady state operation, the voltage V2 generated by the VSC is in phase with V1 (δ=0), so that only reactive power is flowing (P=0). The amount of reactive power transferred between the two sources is given by:

$$Q = \frac{V_1 (V_1 - V_2)}{X} \tag{3}$$

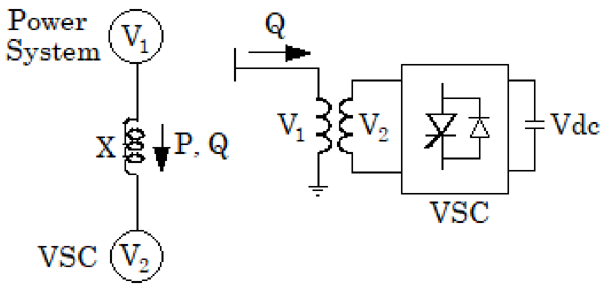


Figure 6
STATCOM principle

If V2 < V1, Q is flowing from power system to the STATCOM. If V2 > V1, Q is flowing from STATCOM to the power system.

Two VSC technologies can be used:

- VSC using GTO-based square-wave inverters. Voltage V2 is directly proportional to voltage Vdc in this particular VSC type. In order to adjust the reactive power, it is necessary to vary the voltage Vdc.
- VSC using IGBT-based PWM inverters. This type of VSC uses a fixed DC voltage Vdc. Voltage V2 is varied by changing the modulation index of the PWM modulator.

The contribution of this paper is to introduce an other technology of SVC to be considered as an alternative solution for improving the power quality. In section 4, a structure of cascaded H-bridge inverter is studied.

# 4. Cascaded h-bridge M-level inverter

## 4.1 Definition

The Cascaded H-bridge M-level Inverter (CHBMLI) is a multilevel inverter that consists of a series association of several H-bridge modules (HBM) or cells. The structure of a three phase CHBMLI is given in Figure 7. The series association of a number s of HBM forms the basic diagram of one phase. Each HBM has its own DC voltage source and four bidirectional switches. "*s*" is the number of HBM by phase (It is also the number of DC voltage sources by phase).

The number of levels is defined by:

$$M = 2 \times S + 1 \tag{4}$$

Example: For a Cascaded H-bridge 7-level inverter, $M = 7$ and $s = 3$

The switches are numbered *Kijk*

where:

"*i*": the HBM number ($i = 1, 2, \ldots\ldots, s$)

"*j*": the phase number ($j = 1, 2, 3$)

"*k*": the switch number ($k = 1, 2, 3, 4$)

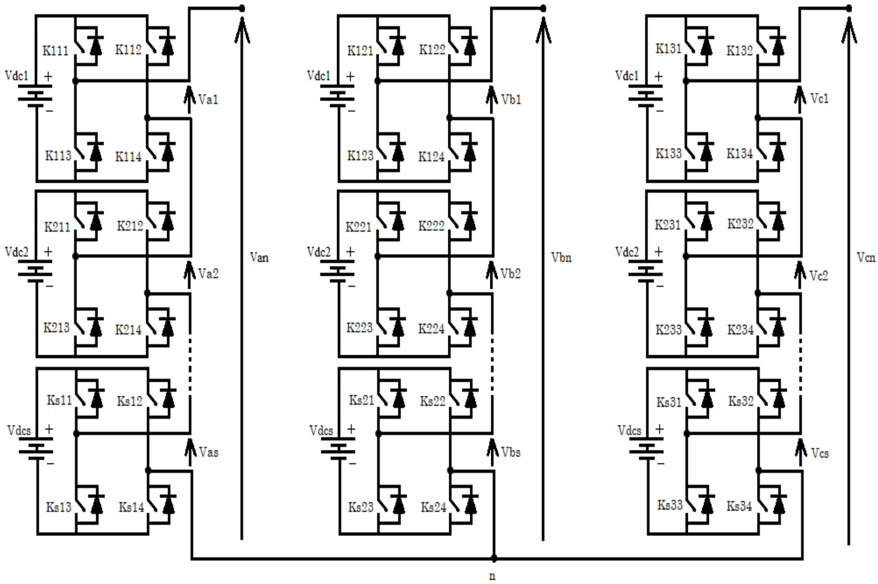


Figure 7
Structure of a three phase CHBMLI

## 4.2 Applications

CHBMLI are used to build a stepped voltage waveform, from a DC voltage source. Their modularity structure facilitates the maintenance. Moreover, it makes it possible to give a very practical way of increasing the number of levels in the system [22]. Due to their capability to ensure the stability of the power system, specifically renewable energy systems, like wind and solar, a contribution of improvement of the performance of the control parameters of a CHBMLI, is proposed in this paper.

## 4.3 Modelling the operation of CHBMLI

Multilevel inverters can be modeled as switched systems, due to the state-dependent dynamics of switching. Switched systems have been extensively studied in the literature, particularly in the context of resilient sampled control under network attacks [23]. The structure of one H-bridge module is given in Figure 8. By different combinations of the four switches, *Kij1: Kij4*, each HBM can generate three different voltage levels: +*Vdci*, -*Vdci* and 0 ("*i*" the HBM number and "*j*" the phase number).

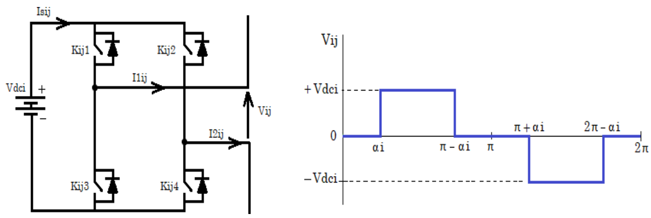


Figure 8
Structure of one H-bridge module (HBM)

The output voltage of one phase in a three phases CHBMLI is the sum of the output voltages of each HBM:

$$\begin{cases} V_{an} = V_{a1} + V_{a2} + \ldots .. + V_{as} \\ V_{bn} = V_{b1} + V_{b2} + \ldots .. + V_{bs} \\ V_{cn} = V_{c1} + V_{c2} + \ldots .. + V_{cs} \end{cases} \tag{5}$$

The output voltage Vij of each HBM depends on its individual DC voltage and the switching angle *αi* of the switch *Kij1*. The switching angles *αi*, are chosen so that the sum of the output voltages forms a stepped voltage waveform. The switching angle must verify the following condition:

$$0 < a_1 < a_2 \ldots\ldots < a_s < \frac{\pi}{2} \tag{6}$$

Figure 9 illustrates the synthesized output voltage of each HBM in a three phase CHBMLI. Phase *b* and phase *c* output voltages are lagging phase *a*, respectively, by 120° and 240°, for the same HBM in each phase.

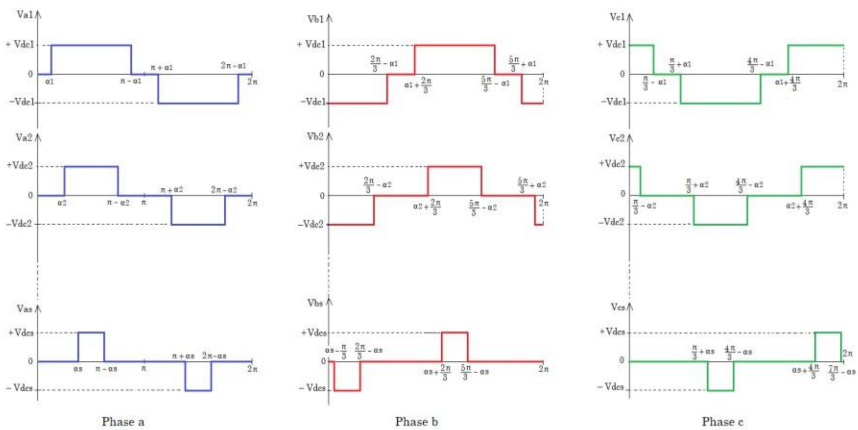


Figure 9
Output voltage of each HBM

In case of a Cascaded H-bridge 7-level inverter (*s* = 3), a twice cycle of the three phase output voltage waveforms synthesized by three different DC voltage sources (*Vdc1* = 54V, *Vdc2* = 52V and *Vdc3* = 53V) are shown in Figure 10. The considered switching angles are *α1* = 20°, *α2* = 45°, *α3* = 70°. Table 1 gives the different combinations of the switches and the corresponding output voltage (*Van*) of phase "*a*". The same principle is applicable for phase *b* and phase *c*.

Table 1

Output voltage and the states of the switches in a Cascaded H-bridge 7-level inverter

| States of the switches | | | | | | | | | | | | Output voltage (*Van*) |
|---|---|---|---|---|---|---|---|---|---|---|---|---|
| *K111* | *K112* | *K113* | *K114* | *K211* | *K212* | *K213* | *K214* | *K311* | *K312* | *K313* | *K314* | |
| On | Off | Off | On | On | Off | Off | On | On | Off | Off | On | *Vdc1+Vdc2+Vdc3* |
| On | Off | Off | On | On | Off | Off | On | Off | Off | Off | Off | *Vdc1+Vdc2* |
| On | Off | Off | On | Off | Off | Off | Off | Off | Off | Off | Off | *Vdc1* |
| Off | Off | Off | Off | Off | Off | Off | Off | Off | Off | Off | Off | *0* |
| Off | On | On | Off | Off | Off | Off | Off | Off | Off | Off | Off | *-Vdc1* |
| Off | On | On | Off | Off | On | On | Off | Off | Off | Off | Off | *-Vdc1-Vdc2* |
| Off | On | On | Off | Off | On | On | Off | Off | On | On | Off | *-Vdc1-Vdc2-Vdc3* |

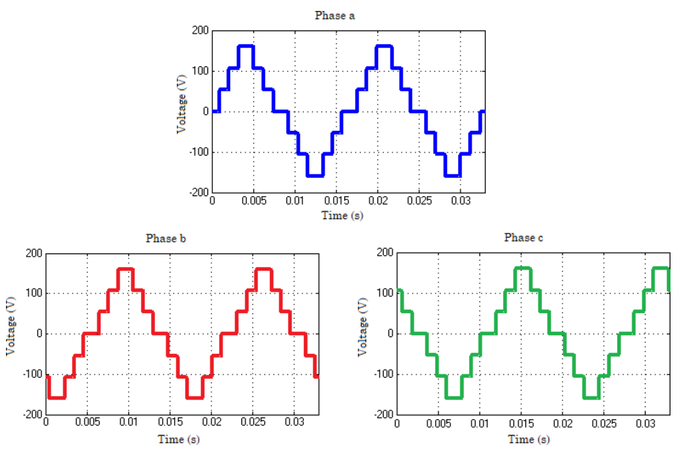


Figure 10

Three phase output voltage waveforms for a 7-level CHB inverter

The rest of this paper aims to find the best switching angles, which will minimize the harmonic distortion of the output voltages in a CHBMLI.

## 4.4 Control model of CHBMLI

The $F_{ijk}$ connection function which translates the open or closed state of the switch "k" is defined by:

$F_{ijk}$ = 1 if the switch is closed and 0 otherwise.

Where,

"*i*": the HBM number ($i = 1, 2, \ldots\ldots, s$)

"*j*": the phase number ($j = 1, 2, 3$)

"*k*": the switch number ($k = 1, 2, 3, 4$)

To maintain the continuity of alternating currents and to avoid the short-circuit of the voltage source, the switches *Kij1* and *Kij3*, *Kij2* and *Kij4*, *Kij1* and *Kij2*, *Kij3* and *Kij4* of each HBM must be checked in a complementary way.

If *αi* the switching angle of the first switch *Ki11* in phase "*a*" of the CHBMLI, the control signals *Bi11* and *Bi12*, respectively, of the switches *Ki11* and *Ki12*, will be:

$$B_{i11} = \begin{cases} 0, & \omega t < a_i \ or \ \omega t > \pi - a_i \\ 1, & \omega t \in \left[ a_i, \ \pi - a_i \right] a_i \end{cases} \tag{7}$$

$$B_{i12} = \begin{cases} 0, & \omega t < \pi + a_i \ or \ \omega t > 2\pi - a_i \\ 1, & \omega t \in \left[ \pi + a_i, \ 2\pi - a_i \right] a_i \end{cases} \tag{8}$$

Where, $w = 2\pi F$ (*F* is the frequency of the output voltage wave). The connection functions *Fi1k* for $k = 1{:}4$, will be:

$$\begin{cases} F_{i11} = B_{i11} \\ F_{i12} = B_{i11} \\ F_{i13} = B_{i11} \\ F_{i14} = B_{i11} \end{cases} \tag{9}$$

Phase "*b*" and phase "*c*" control signals (*Bi21, Bi22 and Bi31, Bi32*) are lagging phase "*a*" (*Bi11, Bi12*), respectively, by 120° and 240° for the same HBM in each phase.

The output voltages *Vai, Vbi* and *Vci* of each HBM-*i* in a three phase CHBMLI are given by the following equation:

$$\begin{cases} V_{ai} = (F_{i11} - F_{i12}) \times V_{dci} \\ V_{bi} = (F_{i21} - F_{i22}) \times V_{dci} \\ V_{ci} = (F_{i31} - F_{i32}) \times V_{dci} \end{cases} \tag{10}$$

*Vai, Vbi* and *Vci* are the HBM-i output voltages, respectively, phase *a*, phase *b* and phase *c*.

Hence the following output voltages *Van*, *Vbn* and *Vcn* of *a* three phase CHBMLI:

$$\begin{cases} V_{an} = \sum_{i=1}^{s} (F_{i11} - F_{i12}) \times V_{dci} \\ V_{bn} = \sum_{i=1}^{s} (F_{i21} - F_{i22}) \times V_{dci} \\ V_{cn} = \sum_{i=1}^{s} (F_{i31} - F_{i32}) \times V_{dci} \end{cases} \tag{11}$$

Here are the voltages between the lines:

$$\begin{bmatrix} U_{AB} \\ U_{BC} \\ U_{CA} \end{bmatrix} = \begin{bmatrix} V_{an} - V_{nb} \\ V_{bn} - V_{nc} \\ V_{cn} - V_{na} \end{bmatrix} \tag{12}$$

If we assume that the simple voltages of the receiver form a balanced three-phase system, we will have:

$$\begin{cases} V_A = V_{AN} = \frac{U_{AB} - U_{CA}}{3} \\ V_B = V_{BN} = \frac{U_{BC} - U_{AB}}{3} \\ V_C = V_{CN} = \frac{U_{CA} - U_{BC}}{3} \end{cases} \tag{13}$$

For currents, if *Isij* denotes the source current of HBM "*i*", phase "*j*" and by *I1ij, I2ij* the output current of the two branches as shown in Figure, we will have:

$$\begin{cases} I_{sia} = F_{i11} \times I_{1ia} + F_{i12} \times I_{2ia} \\ I_{sib} = F_{i21} \times I_{1ib} + F_{i22} \times I_{2ib} \\ I_{sic} = F_{i31} \times I_{1ic} + F_{i32} \times I_{2ic} \end{cases} \tag{14}$$

# 5. Measurement Of Harmonic Distortion

A Fourier series can be used to show any periodic function f(ωt), facilitating the computation of its harmonic components. [6].

$$f(\omega t) = \frac{a_0}{2} + \sum_{n=1}^{\infty} (a_n \cos(n\omega t) + b_n \sin(n\omega t)) \tag{15}$$

When function f(ωt) is periodic in 2π, the coefficients of Eq. (13) are given by:

$$\begin{cases} a_0 = \frac{1}{2\pi} \int_0^{2\pi} f(\omega t).d\omega t \\ a_n = \frac{1}{\pi} \int_0^{2\pi} f(\omega t).\cos(n\omega t).d\omega t \\ b_n = \frac{1}{\pi} \int_0^{2\pi} f(\omega t).\sin(n\omega t).d\omega t \end{cases} \tag{16}$$

In case of a 7-level CHB inverter, where the periodic voltage waveform depends on the switching angles and the individual voltages sources (Figure 11), the corresponding coefficients are given as follows:

$$a_0 = a_n = 0 \tag{17}$$

$$b_n = \frac{4}{n\pi}\left(V_{dc1}\cos(n\alpha_1) + V_{dc2}\cos(n\alpha_2) + V_{dc3}\cos(n\alpha_3)\right)$$

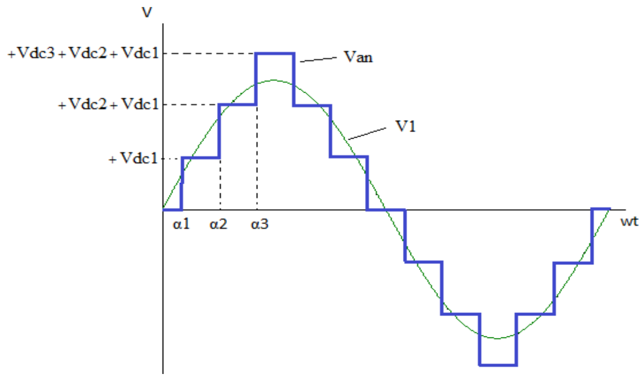


Figure 11

Output voltage of one phase in a cascaded seven-level inverter

Thus, the Fourier analysis, of the output voltage for the seven-level cascaded inverter, can be expressed as follows:

$$V_{an}(\omega t)=\sum_{n=1}^{\infty}\frac{4}{n\pi}(V_{dc1}\cos(n\alpha_1)+V_{dc2}\cos(n\alpha_2)+V_{dc3}\cos(n\alpha_3)).\sin(n\omega t) \tag{18}$$

It may be concluded that the peak amplitude of the sine wave component of the fundamental frequency shown in figure 11 is:

$$b_1=\frac{4}{\pi}(V_{dc1}\cos(\alpha_1)+V_{dc2}\cos(\alpha_2)+V_{dc3}\cos(\alpha_3)) \tag{19}$$

The Root Mean Square (RMS) value of the fundamental component is expressed as:

$$V_{1eff}=\frac{b_1}{\sqrt{2}}=\frac{4}{\sqrt{2}\pi}(V_{dc1}\cos(\alpha_1)+V_{dc2}\cos(\alpha_2)+V_{dc3}\cos(\alpha_3)) \tag{20}$$

And the RMS value of the output voltage is given by:

$$V_{eff}=\sqrt{\frac{1}{2\pi}\int_0^{2\pi}V_{an}}=\sqrt{\frac{2}{\pi}(V_{dc1}^2(\alpha_2-\alpha_1)+(V_{dc1}+V_{dc2})^2.(\alpha_3-\alpha_2)+(V_{dc1}+V_{dc2}+V_{dc3})^2.(\frac{\pi}{2}-\alpha_3)} \tag{21}$$

$\sin(\omega t).d\omega t =$

The best known way used to define the extent of waveform distortion is the distortion factor (DF) given by:

$$DF = \frac{V_{1eff}}{V_{eff}} \tag{22}$$

Where, $V_{1eff}$ and $V_{eff}$ are the rms values, respectively, of the fundamental component and the output voltage.

An alternative measure of the amount of distortion is known as the total harmonic distortion (THD), which is defined as [6] :

$$THD=\sqrt{\frac{V_{eff}^2-V_{1eff}^2}{V_{1eff}^2}}=\sqrt{(\frac{1}{DF})^2-1} \tag{23}$$

Substituting Equations (20) and (21) into Equation (23), the total harmonic distortion can be calculated as follow:

$$THD=\sqrt{\frac{4}{\pi}\frac{(V_{dc1}^2(\alpha_2-\alpha_1)+(V_{dc1}+V_{dc2})^2.(\alpha_3-\alpha_2)+(V_{dc1}+V_{dc2}+V_{dc3})^2.(\frac{\pi}{2}-\alpha_3)}{(V_{dc1}\cos(\alpha_1)+V_{dc2}\cos(\alpha_2)+V_{dc3}\cos(\alpha_3))^2}-1} \tag{24}$$

# 6. Proposed approach

The most frequently employed strategic method in the literature is the elimination of a specific number of order harmonics, while maintaining the fundamental constant. However, this method has a limitation on modulation index over a wide range [13]. Generally, only the higher order harmonics such as the $5^{th}$ and the $7^{th}$ order are concerned. The proposed approach in the present work, aims to define a generalized THD function, which can be considered as an objective function to be minimized by any iterative method. In this section, the THD is first given as function of the switching angles $\alpha_1$, $\alpha_2$,….$\alpha_S$, and the DC voltage $V_{dc1}$, $V_{dc2}$,….$V_{dcS}$, then minimized by a GA.

## 6.1. THD function

THD function that is available for any CHBMLI is defined by generalizing the CHB 7-level case demonstrated in section 4.
For an M-level cascaded inverter with S unequal DC voltage sources, the Fourier analysis given in equation (18), can be generalized as:

$$V_{an}(\omega t)=\sum_{n=1}^{\infty}\frac{4V_{dc}}{n\pi}(K_1\cos(n\alpha_1)+....K_s\cos(n\alpha_s)).\sin(n\omega t) \tag{25}$$

Where, $K_S.V_{dc}$ represents the individual DC voltage sources.
The rms values of the fundamental component $V_{1eff}$ and the output $V_{eff}$ , can be expressed as:

$$V_{1eff}=\frac{4V_{dc}}{\sqrt{2}\pi}(K_1\cos(n\alpha_1)+....K_s\cos(n\alpha_s)) \tag{26}$$

$$V_{eff}=\sqrt{\frac{2V_{dc}^2}{\pi}\sum_{i=1}^{s-1}(\alpha_{i+1}-\alpha_i).(\sum_{k=1}^{i}K_k)^2+(\frac{\pi}{2}-\alpha_s)(\sum_{k=1}^{s}K_k)^2} \quad (27)$$

Therefore,

$$THD=\sqrt{\frac{\pi}{4}\frac{\sum_{i=1}^{s-1}(\alpha_{i+1}-\alpha_i).(\sum_{k=1}^{i}K_k)^2+(\frac{\pi}{2}-\alpha_s)(\sum_{k=1}^{s}K_k)^2}{(K_1\cos(\alpha_1)+K_2\cos(\alpha_2)+...K_s\cos(\alpha_s))^2}-1} \quad (28)$$

## 6.2. Algorithm

The proposed approach aims to minimize the following objective function:

$$F_{abj}=THD=\sqrt{\frac{\pi}{4}\frac{\sum_{i=1}^{s-1}(\alpha_{i+1}-\alpha_i).(\sum_{k=1}^{i}K_k)^2+(\frac{\pi}{2}-\alpha_s)(\sum_{k=1}^{s}K_k)^2}{(K_1\cos(\alpha_1)+K_2\cos(\alpha_2)+...K_s\cos(\alpha_s))^2}-1} \quad (29)$$

Under the constraints:

$$0<\alpha_1<\alpha_2<...<\alpha_s<\frac{\pi}{2} \quad (30)$$

$$1<K_{i(i:1\to s)}<1.2 \quad (31)$$

In the process of determining the minimum THD of the output voltage, the combination switching angles $\alpha_1$, $\alpha_2$,….$\alpha_S$, and the DC voltage $V_{dc1}$, $V_{dc2}$,….$V_{dcS}$, are determined considering the steps summarized below:

**Step 1** Initially a random guess for switching angles *αi* and coefficients *Ki* is done. $V_{dc}$ is taken as 50V and $K_i$ is randomly generated between 1 to 1.2, which make the individual DC voltage sources varying between 50 and 60V.

The GA consists of a population of chromosomes or individuals represented by a combination topology $A_{GA}$ ($\alpha_1$, $\alpha_2$,….$\alpha_S$, $V_{dc1}$, $V_{dc2}$,….$V_{dcS}$). The standard real coded GA is used to find the optimal solution.

**Step 2** The feasibility of each combination topology is checked regarding the constraints given by equation (30) and (31). If one of these constraints is not satisfied, the combination topology will be removed. Otherwise a solution combination topology is defined.

Repeat steps (1) to (2) until the required number of feasible solutions is attained (a population of 100 chromosomes in this study).

**Step 3** The objective function specified in equation (29) is taken into account when evaluating the defined topology through a fitness function..

**Step 4** Selection and reproduction procedure. There is a fitness associated with every chromosome. For the purpose of reproducing, a population will be chosen based on its level of fitness. This research presents a method for selecting superior chromosomes using a roulette wheel.

**Step 5** Crossover is carried out on a subset of the population chosen based on a specified crossover probability.

**Step 6** Mutation. According to the mutation probability, the original state of one or more genes in a chromosome is changed.

During crossover and mutation process (step 5 and 6), the new combination created may be infeasible. Therefore, a random is generated until the feasibility of the new topology is satisfied.

**Step 7** The process restarts with the generation of a new population. Until the maximum number of iterations is reached, the steps (3) through (6) are repeated until they are completed. There is a fixed cap of 100 iterations in this paper.

A flowchart of the suggested plan of action implemented in MATLAB m-file is shown in figure 12.

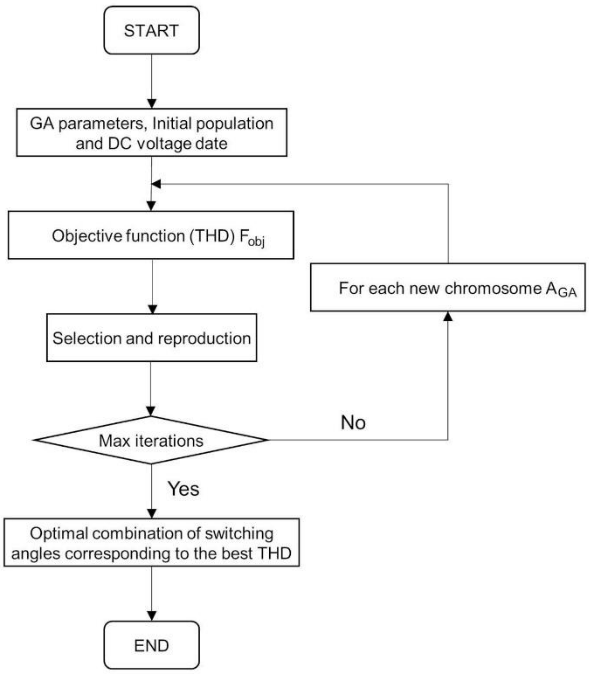


Figure 12.
Proposed approach

# 7. Simulation Results

The simulation results has been carried out in MATLAB environment for a source voltage $V_{dc}$=50V. The switching angles have been randomly selected between 0 and $\pi/2$. The parameters used for the GA are given in table 2.

Table 2

GA parameters

| | |
|---|---|
| Coding variables | Real coding |
| Initial population | 100 |
| Selection | Roulette wheel |
| Crossover probability | 0.8 |
| Mutation probability | 0.02 |
| Maximum number of iteration | 100 |

To evaluate the performances of the developed algorithm, different levels of cascaded H-bridge have been simulated. The results are given in table 3. It only takes about 15 generations for the program to find the best solution.

The output voltage corresponding to the best combination topologies are depicted in figures13, 14, and 15 for the 5-level, 7-level, and 11-level CHB, respectively. The corresponding fundamental phase voltage was synthesized at a frequency of 60 Hz. It's clear that the best configuration confirms the fixed constraints: the switching angles range between 0 and π/2, and the voltage range between 50V and 60V.

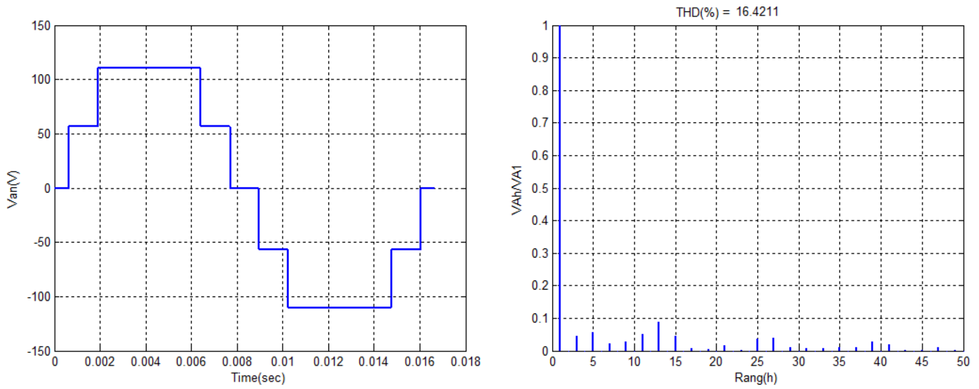


Figure 13

Output voltage Van corresponding to minimum THD and its Spectral analysis in a 5-level CHB

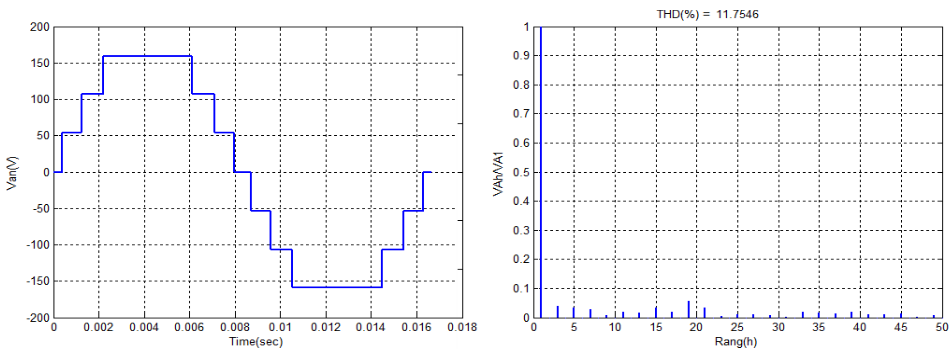


Figure 14

Output voltage Van corresponding to minimum THD and its Spectral analysis in a 7-level CHB

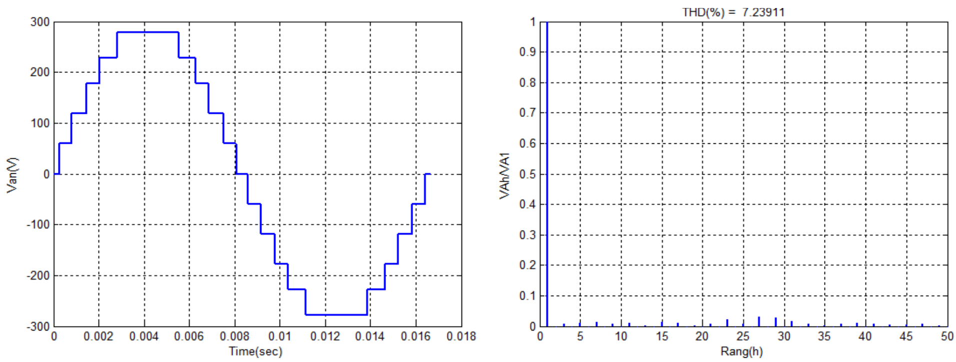


Figure 15

Output voltage Van corresponding to minimum THD and its Spectral analysis in a 11-level CHB

Table 3

Simulation results

| | | 5-level | 7-level | 11-level |
|---|---|---|---|---|
| **Angle *θ* (°)** | $\theta_1$ | 13.4365 | 8.0151 | 5.6899 |
| | $\theta_2$ | 41.2964 | 26.6501 | 17.6431 |
| | $\theta_3$ | - | 47.5873 | 31.4932 |
| | $\theta_4$ | - | - | 43.9951 |
| | $\theta_5$ | - | - | 60.5800 |
| **Voltage *Vdc* (*V*)** | $V_{dc1}$ | 56.7865 | 54.0121 | 59.6939 |
| | $V_{dc2}$ | 54.1680 | 52.4284 | 59.9061 |
| | $V_{dc3}$ | - | 53.0654 | 58.3497 |
| | $V_{dc4}$ | - | - | 50.1676 |
| | $V_{dc5}$ | - | - | 50.9699 |
| **THD (%)** | | 16.42 | 11.75 | 7.24 |

It is seen from the results tabulated in table 3 that a reduction of the total harmonic distortion can be realized by increasing the number of levels. The obtained results are compared to those given in [13] and [15] for a 7-level CHB.

A summary of the comparison can be seen in Table 4. Compared to the results obtained by PIO algorithm given [13], With the approach described in this study, the total harmonic distortion can be reduced by 3.3%. A reduction of up to 35.61% is obtained by comparison with the results given in [15].

Table 4
Comparison of the results for a 7-level CHB

| | | GA presented in this paper | PIO Algorithm [13] | BAT Algorithm [15] |
|---|---|---|---|---|
| Angle *θ(°)* | $\theta_1$ | 8.02 | 12.77 | 7.97 |
| | $\theta_2$ | 26.65 | 26.51 | 17.09 |
| | $\theta_3$ | 47.59 | 55.87 | 35.32 |
| Voltage *Vdc (V)* | $V_{dc1}$ | 1.08xVdc | 1.06xVdc | 1xVdc |
| | $V_{dc2}$ | 1.05xVdc | 1.18xVdc | 1xVdc |
| | $V_{dc3}$ | 1.06xVdc | 1.06xVdc | 1xVdc |
| THD | | 11.75 | 12.15 | 18.25 |

To examine the impact of static compensator device based on CHBMLI, we considered the same Simulink bloc given in Figure 2 with a WS profile that causes a perturbation on the power system as follow: Initially, the WS is set to 8 m/s for the three pairs of WT. Then the WS is rammed, in 3 s after, to 11 m/s starting at $t$ = 1 s for the first pair of WT, at $t$ = 2 s for the second and at $t$ = 3 s for the third pair of WT. The WS goes down to 8 m/s starting at $t$ = 13 s for the first pair, at $t$ = 13.5 s for the second and at $t$ = 14 s for the third pair of WT. The WS perturbation is shown in Figure 16.

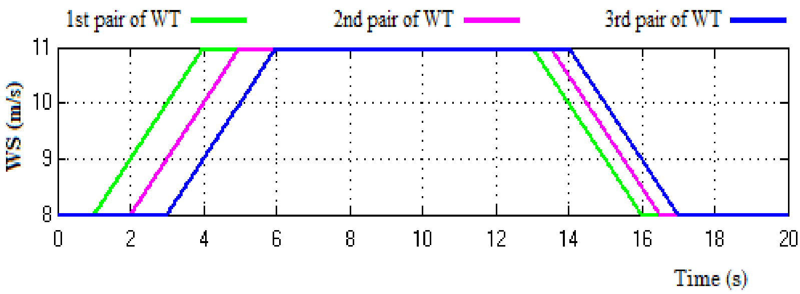


Figure 16
WS perturbation

The simulation results without Static compensator are given in Figure 17. The results show that the active power generated as well as the reactive power absorbed by the wind turbines increases together with the wind speed. The current at low voltage bus in the first pair of turbines is beyond the maximum set to 1.1 pu for more than 10 s. This caused the trip of the first pair of turbines at $t$ = 12.42 s. The AC overcurrent protection has started the trip.

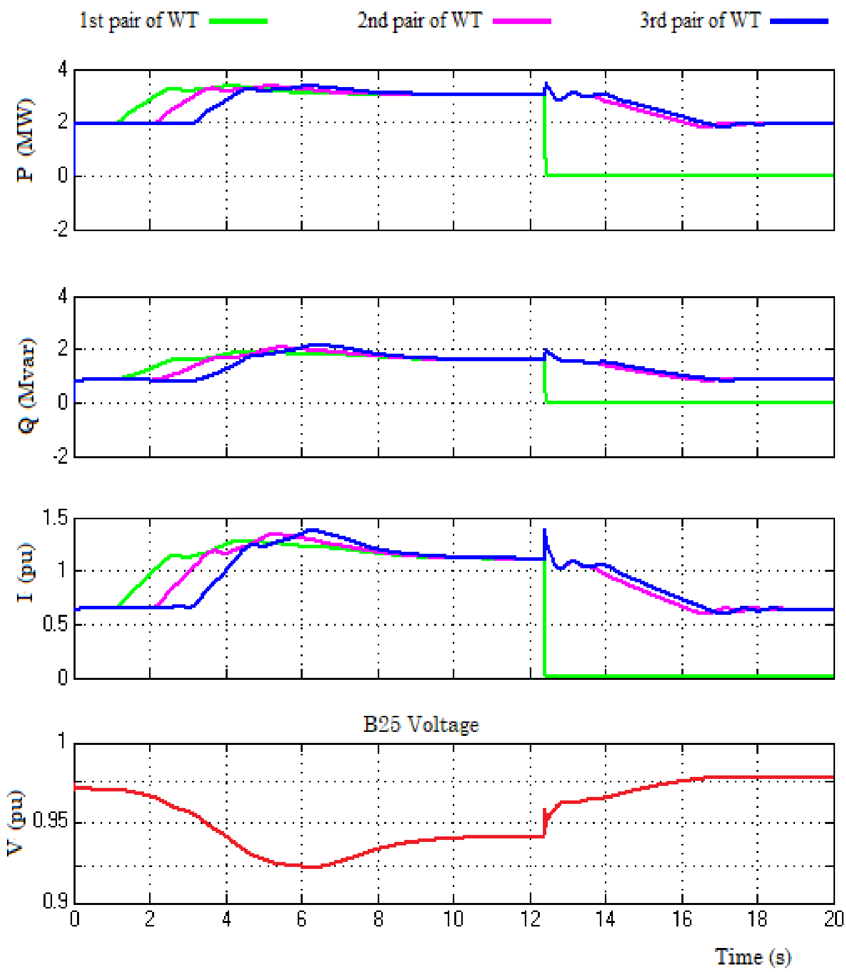


Figure 17
Simulation results without static compensator

Due to the lack of reactive power support, the power system is highly affected by a deep voltage sag observed on bus B25 at $t$ = 6.4 s that is cleared 6 s later when the turbine was tripped.

To maintain the stability of the WTIG and avoid its tripping, a static compensator based on a 7-level CHB inverter is added in the Simulink bloc as shown in figure 18.

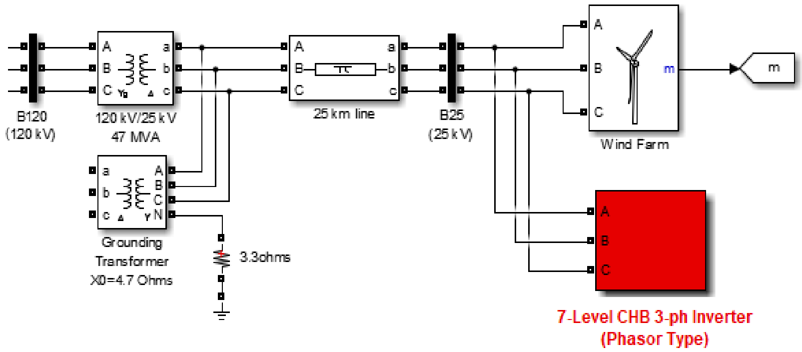


Figure 18

Phasor simulation of a 7-level CHB compensator

The simulation results with static compensator are given in Figure 19. The response of the compensator device for such perturbation is observed through the voltage at bus B25 (Figure 20). As soon as the perturbation detected (at $t$ = 4.8 s), static compensator provides the reactive power required to maintain the 25 kV voltage close to 1 pu at bus B25 throughout the duration of the disturbance. The reactive power absorbed by the WTIG is compensated so that the current at low voltage bus remains below its limit. Therefore, the WTIG can pursue its nominal power generation.

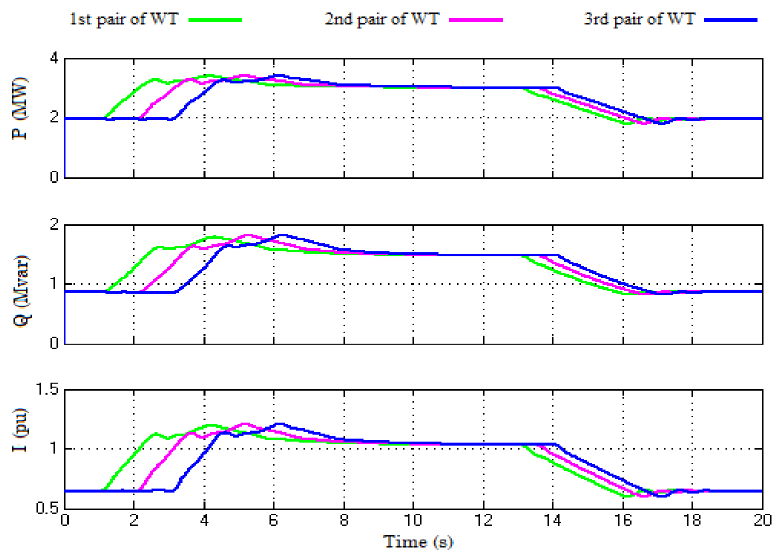


Figure 19

Simulation results with static compensator

The seven-level CHBML that is responsible for the voltage regulating was given a predetermined quantity of reactive power that was necessary in order to keep the WTIG stable. A comparison with the conventional FACTS will be included in the work that will be done in the future. Strategies to regulate the reactive power will also be included.

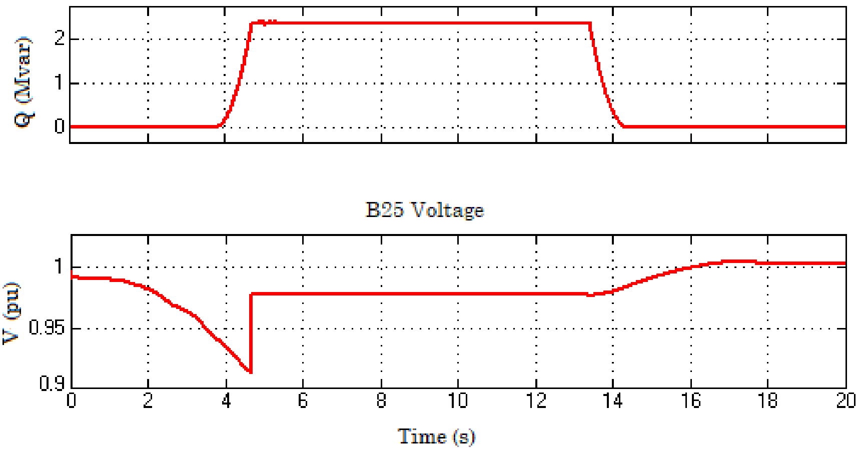


Figure 20
Performance of the 7-level CHB static compensator

## 8. Conclusions

In this article, we have developed a program to minimize the total harmonic distortion by acting on the switching angles of the switches. The performance of the developed approach was verified through different levels of cascaded H-bridge (CHB) inverters (5-level, 7-level and 11-level. The simulation results, obtained using MATLAB m-file, show that the total harmonic distortion could be reduced by comparison with other methods developed in the literature.

## References

[1] Smail, H., Bensafia, Y. (2024) A new approach for load shedding scheme, *Przeglad Elektrotechniczny,* ISSN 0033-2097, N°6, pp 216–218, doi:10.15199/48.2024.06.45.

[2] Smail, H., Alkama, R.,and Medjdoub, A. (2018) Impact of large scale power plant connection on congestion in the algerian electricity transmission system, *Energy*, vol. 159, pp. 115–120, 2018, doi: 10.1016/j.energy.2018.06.076.

[3] Kim, S., Lee, K. (2019) A Modified Third Harmonic Pulse-Width Modulation for Reduced Switching Loss in Cascaded H-Bridge Multilevel

Inverters, *IFAC-PapersOnLine*, vol. 52, no. 4, pp. 472–476, 2019, doi: 10.1016/j.ifacol.2019.08.255.

[4] Laverdure, N. (2005) Sur l'intégration des générateurs éoliens dans les réseaux faibles ou insulaires, *PhD Thesis,* Inst. Natl. Polytech. Grenoble-INPG.

[5] Benmansour, K. (2009) Réalisation d'un banc d'essai pour la Commande et l'Observation des Convertisseurs Multicellulaires Série : Approche Hybride, *Thèse de doctorat*. Université de Cergy-Pontoise. https://theses.fr/2009CERG0403

[6] Zamfirache, IA ,. Precup, RE,. Petriu, EM. (2024) Adaptive reinforcement learning-based control using proximal policy optimization and slime mould algorithm with experimental tower crane system validation, *Applied Soft Computing Journal*, vol, 160, pp. 111–687, doi.org/10.1016/j.asoc.2024.111687

[7] Hentout, A., Maoudj, A., Kouider, A. (2024) Shortest Path Planning and Efficient Fuzzy Logic Control of Mobile Robots in Indoor Static and Dynamic Environments, *Romanian Journal of Information Science and Technology*, vol, 27, N° 1, pp. 21–36

[8] Thakre, K., Barada, K., Sagar, V. (2022) Modified cascaded multilevel inverter for renewable energy systems with less number of unidirectional switches, *Energy Reports*, vol. 8, pp. 5296–5304, doi: 10.1016/j.egyr.2022.03.167

[9] Khounjahan, H., Banaei, MR. (2014) A new low cost cascaded transformer multilevel inverter topology using minimum number of components with modified selective harmonic elimination modulation, *Ain Shams Eng. J.*, vol. 6, no. 1, pp. 67–73, doi: 10.1016/j.asej.2014.08.005

[10] Haidegger, T., Kovács, L., Precup, RE., Benyó, B., Benyó, Z., Preitl, S. (2012) Simulation and control for telerobots in space medicine, Acta Astronautica, Volume 81, Issue 1, Pages 390-402, https://doi.org/10.1016/j.actaastro.2012.06.010

[11] Takács, Á ,. Kovács, L., Rudas, IJ., Emil Precup, R,. Haidegger, T. (2015) Models for Force Control in Telesurgical Robot Systems, *Acta Polytechnica Hungarica*, Vol. 12, No. 8, *DOI: 10.12700/APH.12.8.2015.8.6*

[12] Precup, RE., Bojan-Dragos, CA., Gao, K., Cui, S. (2025) Problem Setting for Trajectory Planning and Cruise Control of a Connected Autonomous Electric Bus in Intersection Scenarios with Human-Driven Vehicles to Optimize Energy, Comfort and Tracking, *Romanian Journal Of Information Science and Technology* , Vol. 28, No. 3, pp. 299–312, DOI: 10.59277/ROMJIST.2025.3.05

[13] Ponnambalam, P., Praveen Kumar., Mayank Varshney M., Choudhary, D., Kalyani, C. (2014) Control of Symmetrical Cascaded Multicell Inverter using Fuzzy Logic, vol. 47, no. 1. *IFAC,* doi: 10.3182/20140313-3-IN-3024.00091

[14] Ahmed, M., Sheir, A., Orabi, M. (2018) Asymmetric cascaded half-bridge multilevel inverter without polarity changer, *Alexandria Eng. J.*, vol. 57, no. 4, pp. 2415–2426, doi: 10.1016/j.aej.2017.08.018

[15] Iqbal, H., Tariq, M., Sarfraz, M., Sarwat, AI., Alhosaini, W. (2022) Selective harmonic mitigation based two-scale frequency control of cascaded modified packed U-Cell inverters, *Energy Reports*, vol. 8, pp. 1009–1020, doi: 10.1016/j.egyr.2022.10.180.

[16] Inverter, H., Mahesh, A., Sandhu, KS. (2018) Evolutionary Algorithm based Optimal Angle strategy for a Cascade, *Procedia Comput. Sci.*, vol. 125, pp. 412–419, doi: 10.1016/j.procs.2017.12.054.

[17] Luo, X., Yi, Z. (2025) Efficiency Management of Engineering Projects Based on Particle Swarm Multi Objective Optimization Algorithm, *Systems and Soft Computing*, 200320, https://doi.org/10.1016/j.sasc.2025.200320.

[18] Ganesan, K., Barathi, K., Chandrasekar, P., Balaji, D. Selective Harmonic Elimination of Cascaded Multilevel Inverter using BAT algorithm, *Procedia Technol.*, vol. 21, pp. 651–657, doi: 10.1016/j.protcy.2015.10.078.

[19] Fri, A., El Bachtiri,.R, Naamane, A. (2014) Triphase symmetrical cascaded multilevel inverter ( 5L ) for PV systems controlled by various multicarrier PWM strategies, *Energy Procedia*, vol. 62, pp. 543–554, doi: 10.1016/j.egypro.2014.12.416.

[20] Kavali, J., Mittal, A. (2016) Analysis of various control schemes for minimal Total Harmonic Distortion in cascaded H-bridge multilevel inverter, *J. Electr. Syst. Inf. Technol.*, vol. 3, no. 3, pp. 428–441, doi: 10.1016/j.jesit.2016.01.007.

[21] Ozpineci, B., Member, S., Tolbert, LM., Member, S. (2005) Harmonic Optimization of Multilevel Converters Using Genetic Algorithms, *IEEE Power Electronics Letters*, vol. 3, no. 3, doi: 10.1109/LPEL.2005.856713.

[22] Housseini, B. (2010) Prototype rapide à base de FPGA d'un algorithme de contrôle avancé pour le moteur à induction. *Maitrise en génie électrique,* Université du Québec. https://depot-e.uqtr.ca/id/eprint/1885.

[23] Zhao, D et al., (2024) Resilient Sampled-Data Event-Triggered Control for Switched Systems Under Denial of Service Attacks, *Acta Polytechnica Hungarica*, vol, 21, N° 10, pp. 263–282, DOI: 10.12700/APH.21.10.2024.10.17.